[Research Paper] 대한금속 · 재료학회지 (*Korean J. Met. Mater.*), Vol. 60, No. 12 (2022) pp.926-932
DOI: 10.3365/KJMM.2022.60.12.926

Transition to n-type Thermoelectric Conduction in Ni-doped $FeSe_2$ Alloys

Young Bin An†, Sang Jeong Park†, Okmin Park, and Sang-il Kim*

Department of Materials Science and Engineering, University of Seoul, Seoul 02504, Republic of Korea

Abstract: We investigated the effect of Ni doping on the electrical, thermal, and thermoelectric transport properties of $FeSe_2$ polycrystalline alloys. $FeSe_2$ alloys exhibit both n-type and p-type conduction at different temperatures and thus their practicality as a thermoelectric material is somewhat limited. In this study, $Fe_{1-x}Ni_xSe_2$ polycrystalline samples with x = 0, 0.01, 0.05, 0.075, 0.1, and 0.125 were synthesized, and it was shown that Ni doping in $FeSe_2$ alloys induces n-type conduction in the entire temperature range. The electrical conductivity is gradually increased with an increase in carrier concentration as Ni doping increases, from 8.52 (x = 0) to 329 S/cm (x = 0.125) at 300 K. The maximum power factor of 0.61 mW/mK^2 was observed in the $Fe_{1-x}Ni_xSe_2$ sample at x = 0.01 at 600 K. Other Ni-doped samples exhibited power factors between 0.31 and 0.34 mW/mK^2 at 600 K. The thermal conductivity gradually decreased from 6.9 (x = 0) to 4.2 W/mK (x = 0.125) with Ni doping because of the additional point-defect phonon scattering of the Ni substitutes. As a result, a zT of 0.11 was observed in x = 0.01 at 600 K, while the zT of the other Ni-doped samples exhibited 0.056-0.069 at 600 K.

(Received 8 August, 2022; Accepted 7 September, 2022)

Keywords: thermoelectric transport, $FeSe_2$

1. INTRODUCTION

Thermoelectric materials have attracted considerable attention as sustainable energy technologies because they can convert a temperature gradient into an electrical potential. Thermoelectric performance is quantified as a dimensionless figure of merit (zT), where high zT values indicate high thermoelectric transfer efficiency. However, improving zT to achieve high thermoelectric performance is challenging. By definition, zT is $\sigma \cdot S^2 \cdot T/\kappa_{tot}$, where σ, S, κ_{tot} and T are the electrical conductivity, Seebeck coefficient, thermal conductivity, and absolute temperature, respectively. $\sigma \cdot S^2$ is referred to as the power factor, and $\kappa_{tot} = \kappa_{elec} + \kappa_{latt}$, where κ_{elec} is the electronic thermal conductivity and κ_{latt} is the lattice thermal conductivity. Therefore, for a high zT, either the power factor ($\sigma \cdot S^2$) should be increased or the thermal conductivity (κ_{tot}) should be decreased [1-3].

To improve $\sigma \cdot S^2$, it is necessary to consider the trade-off relationship between σ and S (i.e., S decreases as σ increases), which leads to the determination of the enhanced power factor. In the case of κ_{tot}, studies have been conducted to reduce the κ_{latt}. In general, the reduction of κ_{latt} is achieved through structural properties such as two-dimensional layered structures or point-defect phonon scattering [4-6]. For Bi-Te-based materials, the two-dimensional layered structure has a Van der Waals gap in the out-of-plane direction; therefore, the thermal conductivity is low, but the electrical conductivity is high in the in-plane direction [7]. However, this structure only materializes in certain compounds despite exhibiting good anisotropy; therefore, point defects have been introduced in thermoelectric alloys via doping or solid solution method to increase phonon scattering [8,9].

Conventional chalcogenides including Bi_2Te_3 have been extensively studied as thermoelectric materials. Chalcogenides have semiconducting properties and exhibit high thermoelectric performance by reducing the thermal conductivity via nanostructuring. In particular, transition-metal dichalcogenides have good optical, electrical, magnetic, and transport properties. In addition, in certain transition metal compounds, the effective mass is sometimes large because of the partially filled electrons in the d and f orbitals, which can

†These authors contributed equally to this work.
- 안영빈 · 박상정: 학부과정, 박옥민: 석사과정, 김상일: 교수
**Corresponding Author:* Sang-il Kim
[Tel: +82-6490-2414, E-mail: sang1.kim@uos.ac.kr]

improve the power factor ($\sigma S^2 \propto m^{*3/2}\mu$), where m^* is the effective mass and μ is the mobility [8-10].

To further enhance thermoelectric performance, both the n- and p-type thermoelectric materials must have similar zT values. Studies have been conducted to improve the transport properties in p-type materials using mechanisms such as impurity doping, solid solution, and vacancy formation in chalcogenide compounds such as GeTe, Cu_2Se, Bi_2Te_3, SnSe, SnTe and $Bi_2Te_{2.7}Se_{0.3}$ [11-16]. Bi-Te based materials exhibit good thermoelectric performance ($zT \approx 1.8$) at room temperature, and the thermoelectric performance of Al-doped Cu_2Se increased to $zT \approx 2.6$ at a high temperature of 1029 K [12,13]. However, improving the thermoelectric performance of n-type materials requires additional investigation.

Recently, the thermoelectric properties of n-type thermoelectric materials have been improved using the structural properties of Zintl or skutterudites. For example, $Ba_{0.3}In_{0.3}Co_4Sb_{12}$, a skutterudite material, has a zT of approximately 1.8 at 850 K and $Mg_{3.02}Y_{0.02}Sb_{1.5}Bi_{0.5}$, a Zintl-type material, has a zT of approximately 1.8 at 773 K, but poor thermoelectric performance at room temperature [17,18].

Fe-based chalcogenides have also been studied as thermoelectric materials [19-21]. Among Fe-based chalcogenides, $FeSe_2$ has good electrical transport properties with a carrier concentration of 10^{18}-10^{19} cm^{-3} [22]. In addition, $FeSe_2$ exhibits a bipolar effect in which the main carrier is inverted at high temperatures [19]. Therefore, obtaining a specific material by enhancing or changing these characteristics is possible.

Based on these conceptualizations, this study was conducted to investigate the electrical and thermoelectric properties of the transition-metal chalcogenide, $FeSe_2$ doped with Ni. The σ, S, Hall carrier concentration, and Hall mobility were measured and the m^* was calculated from the S and Hall carrier concentration.

2. EXPERIMENTAL

To synthesize the reference $FeSe_2$ and Ni-doped $Fe_{1-x}Ni_xSe_2$ (x = 0.01, 0.05, 0.075, 0.1, and 0.125) samples, stoichiometric amounts of Fe, Se, and Ni powders were mixed. The samples were synthesized at 560 K for 72 h via a conventional solid-state reaction. High-purity Fe (99.9%, Alfa Aesar), Se (99.999%, KRTLab), and Ni (99.9%, Alfa Aesar) were loaded in a quartz tube (diameter = 15 mm), which was then vacuum sealed (~10^{-3} Torr). The synthesized ingot was pulverized in a stainless steel container with stainless steel balls using a high-energy ball mill (SPEX 8000D, SPEX) for 5 min to obtain the powders. The bulk sample was fabricated under vacuum (~10^{-5} Torr) by spark plasma sintering (SPS; SPS-1030, Sumitomo Coal Mining Co., Ltd., Tokyo, Japan) at 530°C for 14 min at 75 MPa.

The crystalline phase analysis of the samples was performed using X-ray diffraction (XRD, D8 Discover, Bruker) at 40 kV and 40 mA. The XRD patterns were recorded in the 2θ range of 20°-80° at a scan rate of 0.02° s^{-1} using a Cu K_α source, and the lattice parameter was calculated based on the XRD patterns for each synthesized sample. The thermoelectric properties S and σ were simultaneously measured over a temperature range of 300-600 K in a direction parallel to the SPS pressing direction, using a thermoelectric property measurement instrument (ZEM-3, Advanced-Riko, Yokohama, Japan). The error margins for σ and S were less than 3% and 5%, respectively.

Hall measurements were performed at room temperature in the same direction using the Van der Pauw method to determine carrier concentration (n_H) and mobility (μ_H). The κ_{tot} value of the sample was calculated using the theoretical density (ρ_s), heat capacity (Cp), and thermal diffusivity (λ) ($\kappa_{tot} = \rho_s \cdot C_p \cdot \lambda$). Further, ρ_S of $FeSe_2$ was 7.09 g/cm^3 and C_p was measured using a differential scanning calorimeter (DSC8000, Perkin Elmer, Waltham, USA). The λ value was measured in the temperature range of 300-600 K along the pressing direction, using the laser flash method (LFA457, Netzsch, Selb, Germany). The error margin for λ was less than 7%. Accordingly, zT was evaluated based on data measured in the SPS pressing direction. The error margin for zT would be less than 15%.

3. RESULTS AND DISCUSSION

Figure 1(a) shows the XRD patterns of the synthesized $Fe_{1-x}Ni_xSe_2$ (x = 0, 0.01, 0.05, 0.075, 0.1, 0.125, and 0.2) samples. From the XRD patterns, except for the doping level of x = 0.2, a single phase of $FeSe_2$ with a marcasite structure was confirmed without a Ni-related secondary phase.

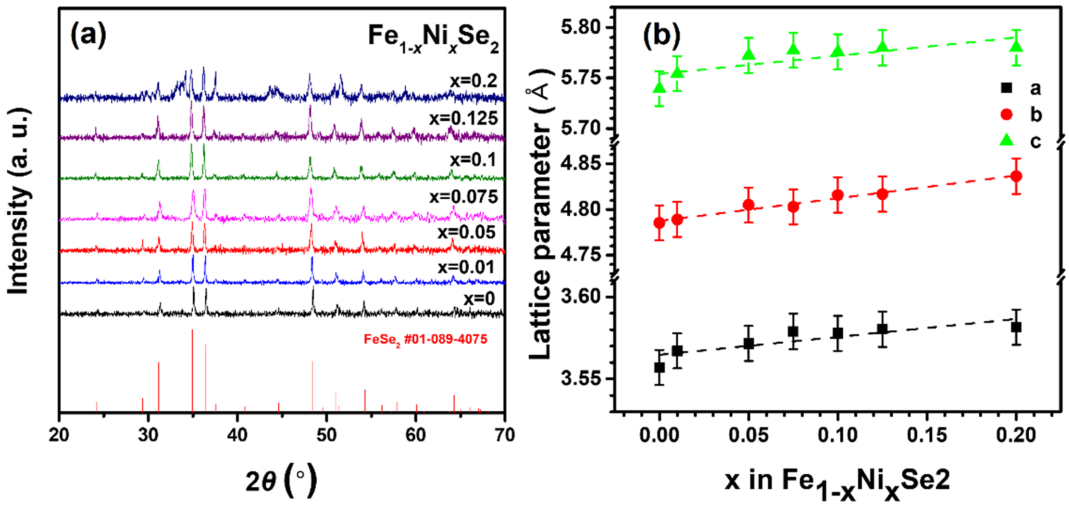

Fig. 1. (a) XRD patterns, and (b) calculated lattice parameters for the $Fe_{1-x}Ni_xSe_2$ (x = 0, 0.01, 0.05, 0.075, 0.1, 0.125 and 0.2) samples.

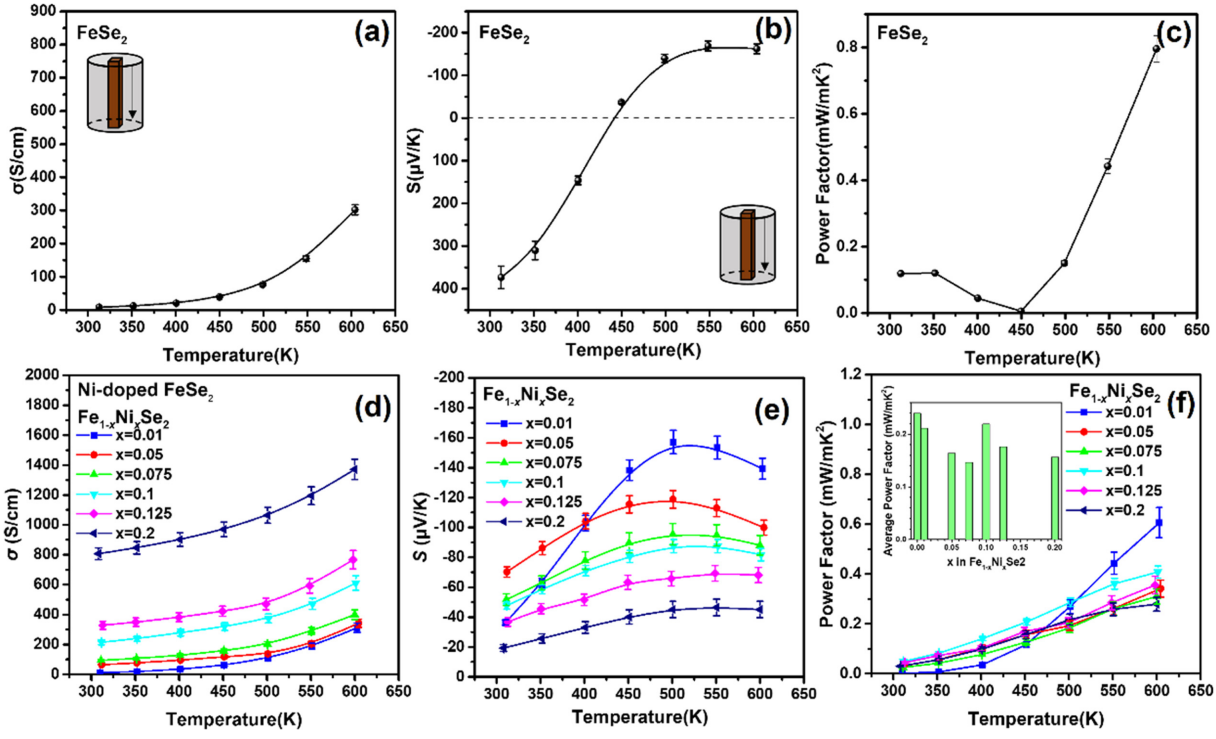

Fig. 2. (a) Electrical conductivity, (b) Seebeck coefficient, and (c) Power factor as a function of temperature for the undoped $FeSe_2$ and (d) electrical conductivity, (e) Seebeck coefficient, and (f) power factor as a function of temperature of the $Fe_{1-x}Ni_xSe_2$ (x = 0.01, 0.05, 0.075, 0.1, 0.125 and 0.2) samples.

However, secondary phases including Fe_2NiSe_4 were observed in the $x = 0.2$ sample, which suggests that the Ni atoms were not well doped in the $FeSe_2$ alloy after doping with $x = 0.2$. Therefore, subsequent measurements were performed, except for the $x = 0.2$ sample. The lattice parameters a, b, and c are shown in Fig. 1(b) and were calculated using the (111), (012), and (121) diffraction peaks. The lattice parameters increased systematically with increasing Ni doping levels. This is because the ionic radius of Ni^{2+} is 0.72 Å, which is larger than that of Fe^{3+} (0.65 Å) [23,24].

Figure 2 shows the measured σ and S values at different

temperatures and the calculated power factor. The σ values (Fig. 2(a)-(d)) systematically increased from 8.52 (undoped) to 328.78 S/cm ($x = 0.125$) at 300 K, with increasing Ni doping level, by approximately 38.6 times. The S plot of the undoped $FeSe_2$ sample (Fig. 2(b)) shows that a bipolar effect occurs, in which the main carrier is reversed between 400 and 450 K, but the Ni-doped samples had no bipolar effect and were converted to n-type semiconductors (Fig. 2(e)).

In addition, the plot of the sample with a doping level x = 0.01 was abnormal; this phenomenon could be caused by the conversion to an n-type semiconductor. That is, it can be described as an intermediate composition converted to n-type. The S values of the $Fe_{1-x}Ni_xSe_2$ samples systematically decreased from -70.31 to -36.71 μV/K at 300 K, from the

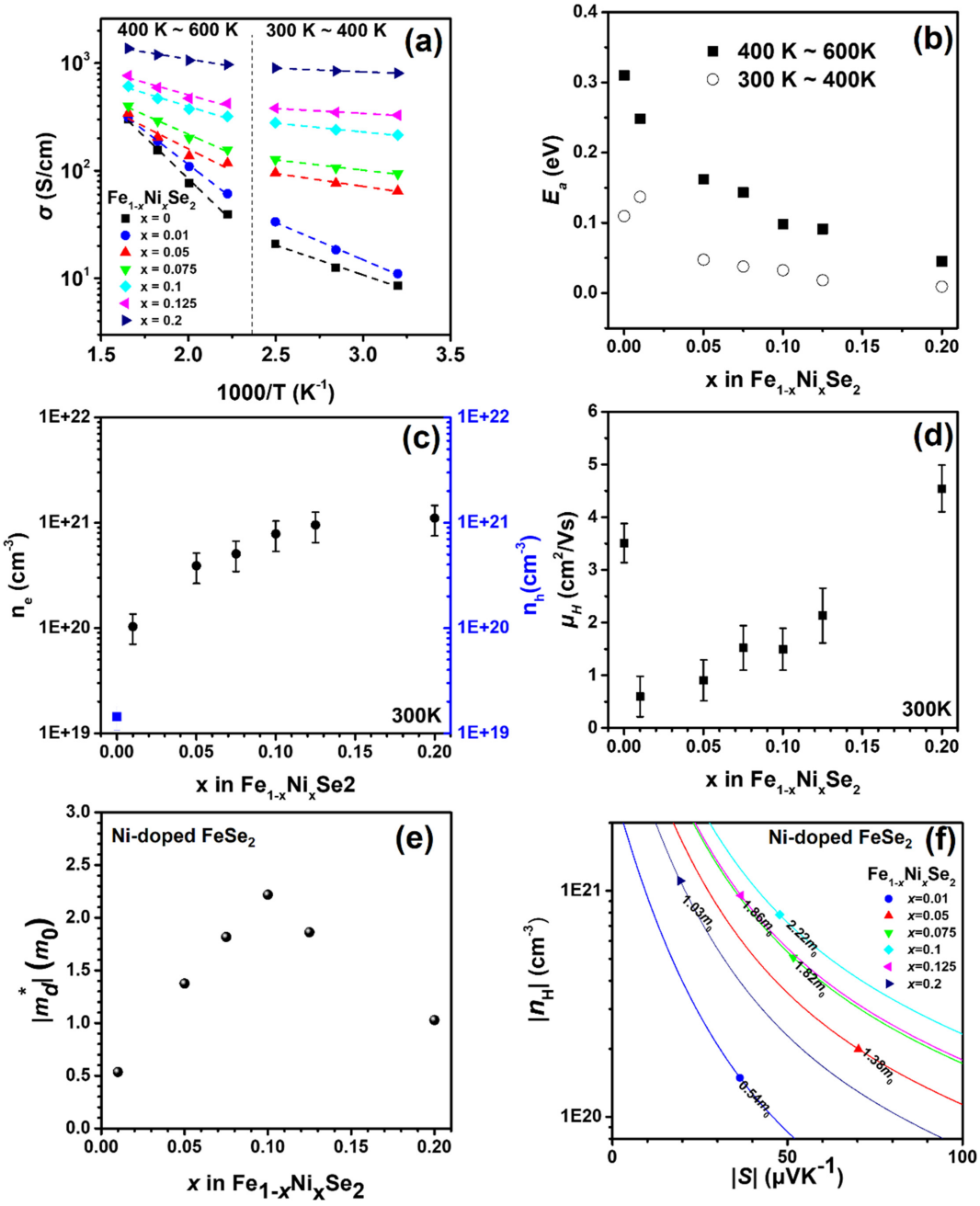

Fig. 3. (a) Logarithmic electrical conductivity as a function of 1000/T. The slope is proportional to the activation energy. (b) Calculated activation energy, (c) Hall carrier concentration, (d) Hall mobility and (e) effective mass, as a function of x for the $Fe_{1-x}Ni_xSe_2$ (x = 0, 0.01, 0.05, 0.075, 0.1, 0.125 and 0.2) samples. (f) S as a function of the measured carrier concentration (Pisarenko plot) at room temperature.

doping level, $x = 0.05$ to $x = 0.125$ due to the trade-off relationship with σ. Consequently, due to the bipolar effect, the power factor of the undoped $FeSe_2$ (Fig. 2(c)) showed the highest values of 0.120 and 0.796 mW/mK^2 at 300 K and 600 K, respectively.

In the case of the power factor of the Ni doped-$FeSe_2$ samples, at 300-500 K, the doping level of $x = 0.1$ showed a maximum value of 0.049-0.287 mW/mK^2, and the power factor of $x = 0.01$ became larger at subsequent temperatures. The average power factor values calculated over the entire temperature range are also shown in the inset of Fig. 2(f). The average power factor had a maximum value at $x = 0.1$, except for undoped $FeSe_2$, which exhibited a bipolar effect.

Figures 3(a) and 3(b) show the logarithmic σ plotted against 1000/T and the calculated activation energy (E_a), respectively. Because E_a is proportional to the negative slope for σ in Fig. 3(a), it was calculated using the Arrhenius relationship, $\sigma \propto \exp(-E_a/kT)$, where k is the Boltzmann constant; the E_a values are plotted for the 300-400 K and 400-600 K temperature ranges. The E_a values gradually decreased with increasing doping levels at all temperature ranges and had higher values at higher temperatures than at lower temperatures.

Figure 3(c) shows the Hall carrier concentration (n_H), where n_H is expressed as the hole concentration (n_h) for undoped $FeSe_2$ and the electron concentration (n_e) for n-type Ni-doped $FeSe_2$. The absolute n_H values of $Fe_{1-x}Ni_xSe_2$ gradually increased from 1.44×10^{19} ($x = 0$) to 9.54×10^{20} cm^{-3} ($x = 0.125$), which suggests that the n_H values systematically increased with doping level. As shown in Fig. 3(d), the μ_H values significantly decreased from 3.51 ($x = 0$) to 0.60 cm^2/Vs ($x = 0.01$) at 300 K due to the significant increase in carrier concentration. However, for doping levels, $x = 0.01$ to $x = 0.125$, μ_H increased systematically at 300 K from 0.60 ($x = 0.01$) to 2.13 cm^2/Vs ($x = 0.125$).

Figures 3(e) and 3(f) show the effective mass and $\log_{10}(n_H)$ as a function of S, at 300 K, for the $Fe_{1-x}Ni_xSe_2$ samples. The solid line in Figure 3(f) was calculated using the following equations for n_H and S for different effective masses:

$$\log_{10}(n_H) = \frac{3}{2}\log_{10}\left(\frac{m_d^* T}{300}\right) + [20.3 - (0.00508 \times |S|) + (1.58 \times 0.967^{|S|})] \quad (1)$$

For all samples, the plots were inferred numerically using Equation (1), and the m_d* values were maximum at $x = 0.1$ [25]. Further, as shown in Fig. 2, the electrical conductivity almost doubled with an increase in doping level from $x = 0.075$ to $x = 0.1$; however, the Seebeck coefficient did not significantly increase. These results indicate that m_d* was modified in favor of S at a doping level of $x = 0.1$.

Figure 4(a) and (b) show the plots of κ_{tot} and κ_{latt}, respectively. the plot of κ_{elec} is given in the inset of Fig. 4(b), where κ_{elec} is calculated using the Wiedemann-Franz equation.

$$\kappa_{elec} = L \cdot \sigma \cdot T \quad (2)$$

where L denotes the Lorenz number. As shown in Fig. 4(a),

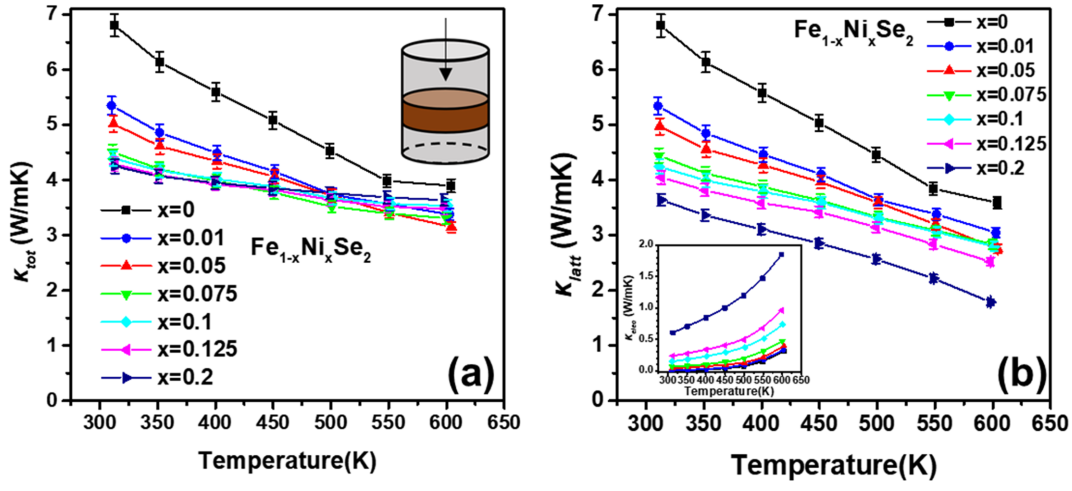

Fig. 4. (a) Total thermal conductivity, (b) lattice thermal conductivity and inset of (b) is electronic thermal conductivity as a function of temperature, for the $Fe_{1-x}Ni_xSe_2$ ($x = 0$, 0.01, 0.05, 0.075, 0.1, 0.125 and 0.2) samples.

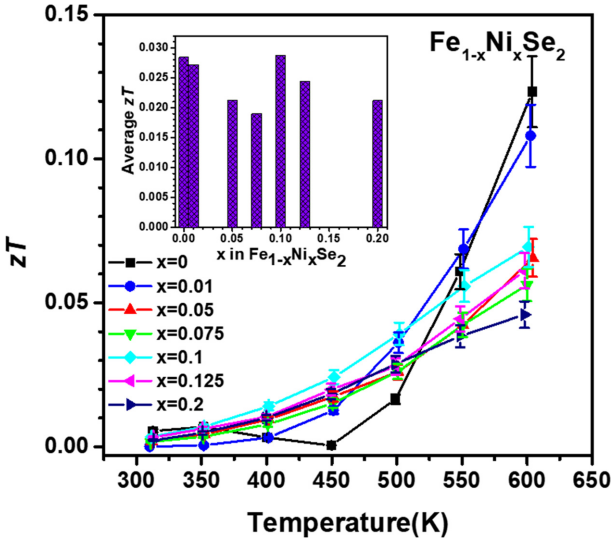

Fig. 5. Thermoelectric figure of merit for the $Fe_{1-x}Ni_xSe_2$ (x = 0, 0.01, 0.05, 0.075, 0.1, 0.125 and 0.2) samples as a function of temperature.

at 300 K, κ_{tot} systematically decreased from 6.81 to 4.29 W/mK, but at temperatures above 500 K, the trend changed because the slope of κ_{tot} increased with increasing doping level.

To elucidate these phenomena, κ_{latt} and κ_{elec} were analyzed. κ_{latt} increased with the doping level and had a greater negative slope in the range of x = 0-0.05 than in the range of x = 0.075-0.125. In addition, κ_{elec} became more significant at higher doping levels. Therefore, according to the thermal conductivity relationship ($\kappa_{tot} = \kappa_{elec} + \kappa_{latt}$), the tendency of thermal conductivity was reversed at high temperatures.

The zT values of the Ni-doped $FeSe_2$ samples were calculated using the experimentally measured values of σ, S and κ_{tot}, and are shown in Fig. 5. A zT of 0.11 was observed at x = 0.01 at 600 K, while the zT of other Ni-doped samples were 0.056-0.069 at 600 K. Even though the maximum zT shown for the pristine $FeSe_2$ sample (x = 0) at 600 K was not further enhanced by the Ni doping, despite the κ_{latt} decrease, the average zT (zT_{avg}) of the sample with x = 0.01 at all temperatures had the highest value of 0.029, as shown in the inset of Fig. 5.

4. CONCLUSIONS

The thermoelectric properties of Ni-doped $Fe_{1-x}Ni_xSe_2$ (x = 0, 0.01, 0.05, 0.075, 0.1, and 0.125) alloys were analyzed. Ni doping in $FeSe_2$ alloys induced n-type conduction over the entire temperature range, as $FeSe_2$ alloys exhibited both n-type and p-type conduction at different temperatures. Further, the electrical conductivity increased by approximately 40 times, from 8.52 (x = 0) to 329 S/cm (x = 0.125), with the increase in carrier concentration. In addition, the activation energy decreased with increasing doping levels, and the effective mass was maximized at x = 0.1. Therefore, the average power factor at x = 0.1 had the highest value except for undoped $FeSe_2$. The total thermal conductivity was decreased by Ni doping, from 6.81 to 4.29 W/mK, while the lattice thermal conductivity also decreased. Consequently, the sample with x = 0.1 had the highest average zT of approximately 0.029.

ACKNOWLEDGEMENTS

This study was supported by the National Research Foundation of Korea (NRF-2019R1C1C1005254, and NRF-2022R1F1A1063054).

REFERENCES

1. G. D. Mahan and J. O. Sofo, *Proc. Natl. Acad. Sci.* **93**, 7436 (1996).
2. Z. Huang, D. Wang, C. Li, J. Wang, G. Wang, and L. Zhao, *J. Mater. Chem. A*. **8**, 4931 (2020).
3. P. G. Klemens, *Int. J. Thermophys.* **2**, 55 (1981).
4. S. Manzeli, D. Ovchinnikov, and D. Pasquier, *Nat. Rev. Mater.* **2**, 17033 (2017).
5. B. Poudel, Q. Hao, Y. Ma, Y. Lan, A. Minnich, B. Yu, X. Yan, D. Wang, A. Muto, D. Vahaee, Z. Chen, J. Liu, M. S. Dresselhaus, G. Chen, and Z. Ren, *Science* **320**, 634 (2008).
6. Z. G. Chen, G. Han, L. Yang, L. Cheng, and J. Zou, *Prog. Nat. Sci.* **6**, 535 (2012).
7. J. A. Wilson and A. D. Yoffe, *Adv. Phys.* **18**, 193 (1969).
8. K. H. Lee, Y. Kim, D. H. Kim, C. O. Park, H. S. Kim, and S. I. Kim, *J. Mater. Res. Technol.* **15**, 4781 (2021).
9. K. H. Lee, H. S. Kim, S. S. Choo, W. H. Shin, J. H. Lim, S. W. Kim, and S. I. Kim, *Scr. Mater.* **186**, 357 (2020).
10. B. Xu, M. T. Feng, T Agne, L. Zhu, X. Ruan, G. J. Snyder, and Y. Wu, *Angew. Chem. Int. Ed.* **56**, 3546 (2018).
11. K. S. Bayikadi, C. T. Wu, L. C. Chen, K. H. Chen, F. Chou, and R. Sankar, *J. Mater. Chem. A* **8**, 5332 (2020).
12. B. Zhong, Y. Zhang, W. Li, Z. Chen, J. Cui, W. Li, Y. Xie,

Q. Hao, and Q. He, *Appl. Phys. Lett.* **105**, 123902 (2014).
13. S. D. Bhame, D. Pravarthana, W. Prellier, and J. G. Noudem, *Appl. Phys. Lett.* **102**, 211901 (2013).
14. S. Li, Y. M. Wang, C. Chen, X. F. Li, W. H. Xue, X. Y. Wang, Z. W. Zhang, F. Cao, J. H. Sui, X. J. Liu, and Q. Zhang, *Adv. Sci.* **5**, 1800598 (2018).
15. M. Rakshit, M. Jana, and D. Banerjee, *J. Mater. Chem. A* **10**, 6872 (2022).
16. Y. S. Lim, B. G. Park, and G. G. Lee, *Korean J. Met. Mater.* **58**, 334 (2020).
17. W. Zhao, Z. Liu, Z. Sun, Q. Zhang, P. Wei, X. Mu, H. Zhou, C. Li, S. Ma, D. He, P. Ji, W. Zhu, X. Nie, X. Su, X. Tang, B. Shen, X. Dong, J. Yang, Y. Liu, and J. Shi, *Nature* **549**, 247 (2017).
18. S. W. Song, J. Mao, M. Bordelon, R. He, Y. M. Wang, J. Shuai, J. Y. Sun, X. B. Lei, Z. S. Ren, S. Chen, S. Wilson, K. Nielsch, Q. Y. Zhang, and Z. F. Ren, *Mater. Today Phys.* **8**, 25 (2019).
19. G. Li, B. Zhang, J. Rao, D. H. Gonzalez, G. R. Blake, R. A. de Groot, and T. T. M. Palstra, *Chem. Mater.* **27**, 8220 (2015).
20. F. F. Aliev, G. G. Guseinov, G. P. Pashaev, G. M. Agamirzoeva, and A. B. Magerramov, *Inorg. Mater.* **44**, 115 (2008).
21. O. Park, T. W. Kim, S. W. Lee, H. S. Kim, W. H. Shin, J. U. Rahman, and S. I. Kim, *Korean J. Met. Mater.* **60**, 315 (2022).
22. D. K. Sharma, B. Joshi, K. R. Patel, V. Ganeshan, and Y. K. Sharma, *Int. J. Rec. Res. Rev.* **6**, 22 (2013).
23. R. Kayestha, Sumati, and K. Hajela, *FEBS Lett.* **368**, 285 (1995).
24. N. Pathak, S. K. Gupta, K. Sanyal, M. Kumar, R. M. Kadam, and V. Natarajan, *Dalton Trans.* **43**, 9313 (2014).
25. K. H. Lee, H. S. Kim, S. S. Choo, W. H. Shin, J. H. Lim, S. W. Kim, and S. I. Kim, *Scr. Mater.* **186**, 357 (2020).